Environmental Science and Pollution Research (2020) 27:10966–10980
https://doi.org/10.1007/s11356-019-06674-x

RESEARCH ARTICLE

Photodegradation of 4-nitrophenol over B-doped TiO_2 nanostructure: effect of dopant concentration, kinetics, and mechanism

Vandana Yadav[1] · Priyanka Verma[1] · Himani Sharma[2] · Sudhiranjan Tripathy[3] · Vipin Kumar Saini[1]

Received: 8 May 2019 / Accepted: 1 October 2019 / Published online: 17 January 2020

Abstract

The 4-nitrophenol (4-NP) is one of the carcinogenic pollutants listed by US EPA and has been detected in industrial wastewater. This study investigates the photocatalytic degradation of 4-NP with TiO_2 and boron (B)-doped TiO_2 nanostructures. The degradation on undoped and B-doped TiO_2 with various boron loadings (1–7%) was studied to establish a relationship between structure, interface, and photo-catalytic properties. The results of XRD, micro Raman, FTIR, and HRTEM show that the B doping has improved the crystallinity and induces rutile phase along with anatase (major phase). The N_2 adsorption-desorption, SEM-EDX, and XPS indicated that the B induced the formation of mesoporous nanostructures in TiO_2 and occupies interstitial sites by forming Ti-O-B type linkage. The surface area of pure TiO_2 was decreased from 235.4 to 63.3 m^2/g in B-TiO_2. The photo-physical properties were characterized by UV-Vis DRS, which showed decrease in the optical band-gap of pure TiO_2 (2.98 eV) to B-TiO_2 (2.95 eV). The degradation results demonstrated that the B doping improved the photocatalytic activity of TiO_2; however, this improvement depends on the B concentration in doped TiO_2. B-doped TiO_2 (> 5% B) showed 90 % degradation of 4-NP, whereas the undoped TiO_2 can degrade only 79 % of 4-NP. The degradation followed pseudo-first-order kinetics with rate constant values of 0.006 min^{-1} and 0.0322 min^{-1} for pure TiO_2 and B-TiO_2 respectively. The existence of a reduced form of Ti^{3+} on the surface of TiO_2 (as evidence from XPS) was found responsible for enhancement in photocatalytic activity.

Keywords Photo-catalysis · Kinetics · Mechanism · 4-Nitrophenol · Degradation pathway · TiO2 nanostructure · Doping

Introduction

In the current perspective, the heterogeneous photocatalysis has been considered as one of the economic, energy-efficient, and clean technology for removal of organic compounds such as amoxicillin, tetrodotoxin, ketamine, gentamicin, carbophenothion, ofloxacin, erythromycin, enrofloxacin, lidocaine, and ciprofloxacin from wastewater (Fakhri and Khakpour 2015; Fakhri and Naji 2017, 2016; Mohammadi et al. 2016; Fakhri and Kahi 2017; Fakhri et al. 2015, 2016; Fakhri and Behrouz 2015a, b; Hassani et al. 2018a, b, 2016). Heterogeneous photocatalysis utilizing titanium oxide (TiO_2) semiconductor as a photocatalyst is more efficient environmental cleanup technique in comparison to conventional techniques. In this process, there is no residue after degradation of contaminant or pollutant, as it slowly breaks down the large contaminant molecules. Therefore, the process of sludge disposal to landfill is not anymore required. Photocatalysis is also suitable for decomposition of organic and inorganic compounds at very low concentrations ranging from 0.01 to 10 mg/L. The catalyst used in the photocatalytic process can be reused because it does not consume and remains unchanged (Hassani et al. 2018a, b, Byrne et al. 2018).

Responsible Editor: Suresh Pillai

Electronic supplementary material The online version of this article (https://doi.org/10.1007/s11356-019-06674-x) contains supplementary material, which is available to authorized users.

✉ Vipin Kumar Saini
vksaini.senr@doonuniversity.ac.in

[1] School of Environment & Natural Resources, Doon University, Dehradun, Uttarakhand 248001, India

[2] Department of Physics, Doon University, Dehradun, Uttarakhand 248001, India

[3] Institute of Materials Research and Engineering, A*STAR (Agency for Science, Technology and Research), 2 Fusionopolis Way, Innovis, #08-03, Singapore 138634, Singapore

Titanium oxide (TiO_2) is of considerable industrial importance for photocatalytic applications due to its properties like low cost, chemical inertness, non-toxicity, and photo stability (Linsebigler et al. 1995). Its practical applications include self-cleaning surfaces, wastewater, and air purification, bacteria inactivation, H_2 production *via* photocatalytic water splitting, and photo conversion of CO_2 to methane or other lower hydrocarbons (Kumaravel et al. 2019; Hashimoto et al. 2005). However, its large-scale technological applications are limited because of its wide band gap (3.0–3.2 eV), low photonic yield, and high recombination rate of the electron-hole pair (Ward and Bard 1982). Due to the large band gap, this oxide can only utilize a small fraction of sunlight (> 5%) in ultra-violet (UV) region ($\lambda < 387$ nm). Whereas, visible light ($\lambda > 400$ nm) constitutes the major fraction (45%) of sunlight reaching to the earth surface (Ren et al. 2007). These limitations have opened a new domain of research for researchers as how to extend or shift the absorption spectra of TiO_2 from UV to visible region. Many researchers have reported that any change or shift in the spectral response of TiO_2 from UV to the visible region will also result in a significant increase in its photocatalytic activity (PCA).

Several approaches like encapsulation, functionalization, dye sensitization, complexation, doping, capping, surface modification, coupling with another semiconductor, and incorporation with other nanomaterials have been explored by researchers to extend the optical response of TiO_2 (Shipra and Manoj 2011). Among them, doping is one of the efficient methods for inducing visible light activity (VLA) in TiO_2. The very first attempt of doping in TiO_2 with transition-metal was reported by Chio and co-workers in 1994 (Chio et al. 1994). However, metal doping has some limitations, because quite often, the metal dopant acts as an electron trap, and thus decreases the photocatalytic activity and sometimes causes thermal instability. As a result, many researchers have initiated to utilize non-metal dopants such as C, N, S, B, F, and I to improve photoactive properties of TiO_2 (Ren et al. 2007; Viswanathan and Krishanmurthy 2012; Hamadanian et al. 2009; Xu et al. 2009; Park and Choi 2004; Hong et al. 2005). The addition of non-metal into TiO_2 lattice results in mixing of the p states of the non-metal with the O-2p states that shifts the valence band edge upwards and thereby decreases the band gap. Due to this reason, the non-metal-doped TiO_2 has proved to be a more efficient catalyst for photocatalytic degradation of organic pollutants.

Amongst non-metallic dopant, boron is quite an important dopant. Studies have reported that boron doping into TiO_2 lattice has resulted in enhanced photocatalytic activity (Stengl et al. 2010; Zaleska et al. 2008). Zaleska et al. synthesized B-doped TiO_2 catalysts through the sol-gel method and by grinding anatase powder with a dopant (Zaleska et al. 2008). They used boric acid triethyl ester and boric acid as boron sources and evaluated the photocatalytic activity of the prepared B-TiO_2 catalysts through the degradation of phenol under UV and visible light irradiation. B-TiO_2 prepared by grinding of anatase powder with boric acid triethyl ester exhibited better photoactivity under visible light as compared to that of pure TiO_2. They further prepared B-TiO_2 photocatalysts by surface impregnation method using boric acid triethyl ester as a boron precursor and observed that boron forms B-O-Ti species on the surface of TiO_2 grains (Zaleska et al. 2009). Chen et al. (2006) observed that B-doped TiO_2 has higher photocatalytic activity than pure TiO_2 in a photocatalytic regeneration of nicotinamide adenine dinucleotide. They attributed this enhancement due to the formation of Ti^{3+}, which facilitates the separation of excited electrons and holes pairs and also slows down their recombination rate. Sol-gel method is frequently used for in situ doping of B into TiO_2 lattice. Lozano and co-workers prepared a series of boron-doped TiO_2 photocatalysts (2% B-TiO_2) with different water/alkoxide molar ratios through sol-gel method. Their study showed that degradation of Orange II azo dye increases with surface area, particle size, boron, and water content in photocatalyst (May-Lozano et al. 2014). A modified sol-gel method was used by Zhang et al. (2012) for the synthesis of boron-doped TiO_2. The catalysts were calcined at a temperature ranging from 300 to 600 °C and the 3% B-TiO_2 catalyst calcined at 400 °C showed 96.7% degradation of methyl orange under UV irradiation.

In the context of water pollution, 4-nitrophenol (4-NP) is a toxic, anthropogenic, inhibitory, and refractory organic compound. It is used extensively in chemical industries for the manufacturing of pesticides, pharmaceuticals, and synthetic dyes (Kavitha and Palanivelu 2005). As a result, it is one of the common pollutants present in industrial wastewater. According to the U.S. Environmental Protection Agency (U.S. EPA 1980), it is carcinogenic and can damage the central nervous system, liver, kidney, and blood of humans and animals. Various conventional methods like catalytic wet-air-oxidation, biological degradation, adsorption, UV-oxidation, nano-filtration, and coagulation–flocculation have been used for the treatment of wastewater, containing 4-NP. Most of these methods cannot degrade 4-NP, due to its high stability and solubility in water. Furthermore, most of these methods transfer the pollutant from one phase to another and do not provide an ultimate solution. However, the 4-NP can be reduced in the presence of suitable catalyst while using the strong reducing agent like sodium borohydride but the process is not economical as it requires the use of expensive reducing agent (Kamal et al. 2019a, b; Khan et al. 2017; Haider et al. 2016; Ali et al. 2017a, b, 2018). Thus, it is important to develop a more efficient and complete method for its remediation from wastewater before being discharged.

With this background, we believe that B-doped TiO_2 can be a suitable material for photocatalytic degradation (PCD) of 4-NP. To the best of our knowledge, the potential of boron-

doped TiO_2 catalyst for photodegradation of 4-NP has not been studied so far. Therefore, in this work, we have performed the PCD studies of 4-NP using pure TiO_2 and B-doped TiO_2. The undoped and boron-doped TiO_2 catalysts were synthesized through sol-gel route using titanium isopropoxide (TTIP) and boric acid (BA) as precursors for titanium oxide and boron respectively. The physicochemical and photophysical properties of the photocatalyst were investigated using various characterization techniques such as surface area and pore analysis, XRD, UV-Vis, FTIR, SEM-EDX, HRTEM, micro Raman spectroscopy, and XPS. The effect of various parameters like irradiation time, catalyst dose, and dopant concentration on PCD of 4-NP was studied. The kinetic modeling of photocatalytic degradation data was also performed to co- relates the effect of boron doping on PCD kinetics

Materials and methods

Synthesis of photocatalysts

The reagents used in this study are titanium isopropoxide (TTIP, Sigma-Aldrich, 99% purity), absolute ethanol (Merck, 99% purity), and boric acid (SRL, 99.5% purity). Pure commercial TiO_2 (P25) was also purchased (Rankem, 99% purity) for comparison purpose and referred as TiO_2C in the following text. The boron-doped TiO_2 was prepared through sol-gel method, involving homogeneous hydrolysis of TTIP in ethanol and water as described elsewhere (Ellappan et al. 2014). Briefly, solution A was prepared by dispersing 8 ml of TTIP in 42 ml of ethanol followed by 30 min of stirring. Meanwhile, solution B was prepared by mixing ethanol (50 ml) and water (50 ml) (Merck Millipore) in a 1:1 v/v ratio. Then, 100 ml of solution B was added dropwise into solution A at 80 °C and continuously stirred for 60 min. After that, 10 ml of boric acid solution (1% w/v) in water was added dropwise to the mixture of solution A and B. The solution was further stirred for 30 min at 80 °C. The resulting milky suspension was kept aside for aging, for 24 h. After aging, the white precipitate was settled down at the bottom, which was dried in an oven at 120 °C for 12 h (or till complete dry). Finally, the dried material was ground and then calcined at 400 °C in air for 4 h using a heating rate of 3 °C/min. The so-obtained boron-doped TiO_2 was ascribed as BT1 in the following experiments. Two more B-TiO_2 samples were prepared similarly, by adding 5% and 7% w/v solutions of boric acid, and were denoted as BT5 and BT7, respectively. The TiO_2 without doping was prepared in a similar manner but without adding boric acid and it is referred as undoped TiO_2.

Characterization of photocatalysts

The structural characterization of prepared catalysts was carried out using powder X-ray diffraction instrument (XRD-Philips X'Pert diffractometer) equipped with Cu-Kα radiation, operating in 2θ mode. The samples were analyzed in the range of 20°–80°. The Raman spectra of prepared samples were recorded using a Jobin Yvon Lab Ram HR 800 setup equipped with a 488 nm Ar ion laser excitation line. The band gap of prepared samples was calculated with UV-Vis absorption spectroscopic measurements, and carried out on a UV-Vis diffuse reflectance spectrophotometer (Shimadzu UV-2550) in the range of 200–800 nm, where the absorption spectra were referenced to $BaSO_4$. The Brunauer-Emmett-Teller (BET) surface area of the samples (degassed for 60 min at 150 °C) was determined from low-temperature nitrogen adsorption-desorption isotherms using Micromeritics instrument (ASAP-2020 model). The pore size distribution (pore diameter and pore volume of samples) was determined by the Barrett-Joyner-Halenda (BJH) method. Fourier-transform infrared (FTIR) spectra of the samples were recorded on a spectrometer WQF-410 (Bruker), where the sample powders were mixed with KBr to prepare pellets and then spectra were recorded in the wavenumber range of 4000–400 cm^{-1}. The morphology of the samples was observed using scanning electron microscopy (SEM-FEI Quanta 200FSEM, Hillsboro), that was equipped with energy-dispersive X-ray (EDX). The internal structure and d-spacing of the samples were analyzed out using high-resolution transmission electron microscopy (TEM- JEOL TEM Model 2100). For TEM analysis, the powdered samples are dispersed in isopropanol solvent for homogeneous dispersion and then the copper grids are dipped into it and dried. Then, the grids are placed on the specimen holder, which is to be loaded inside the TEM instrument for imaging. The chemical states of prepared materials were examined using an X-ray photoelectron spectrometer (XPS-Thermo Scientific Theta Probe Escalab 250, a monochromatic Al Kα X-ray source). Detailed scans were recorded for B1s, O1s, and Ti2p and all the binding energies were referenced to the C1s peak (284.6 eV).

Photocatalytic degradation studies

The photocatalytic efficiency of doped and undoped photocatalyst was evaluated by degradation of 4-NP under UV light irradiation. The photocatalysis experiments were performed in a cylindrical batch reactor (500 mL), made up of quartz glass (Lelesil Innovative Systems Ltd. Mumbai, India). The reactor was equipped with a water jacket to control the temperature at about 20 °C. The photo-irradiation was performed with a 125-W mercury lamp, emitting a wavelength of 354 nm as the UV light source.

In every experiment, before irradiation, 150 mL of 4-NP aqueous solution of variable concentration, containing the required amount of catalyst, was stirred continuously in the dark for 30 min to reach adsorption equilibrium. In order to determine the adsorption capacity of the catalyst, about 5 ml of sample was withdrawn at that time by syringe for analysis. Subsequently, the reaction mixture was continuously stirred under UV light, and 5 ml of aliquots was withdrawn at fixed intervals of time up to 3 h. The aliquots were filtered through a Millipore syringe filter (pore size 0.45 μm) to remove the photocatalyst. The concentration of remaining 4-NP in filtered solution was determined by measuring the aborbance using UV-Vis spectrophotometer (Thermo Scientific, Evolution 201) at $\lambda_{max} = 316$ nm. Throughout this photocatalytic study, the experiments were carried out in duplicates, and wherever required, the experiments were repeated up to three times. The uncertainty of the experiments as estimated by the repeatability of the experiments was found below ± 2% and had no significance influence on the interpretation of the results.

Results and discussion

Structural characterization

X-ray diffraction (XRD) technique was used to analyze the alteration in crystallographic phases, before and after boron doping. The XRD pattern of the samples is presented in Fig. 1a. The average crystallite sizes of the samples were determined using following Scherrer equation (Scherrer 1918):

$$D = \frac{K\lambda}{\beta Cos\theta} \quad (1)$$

Where, K = 0.89 is shape factor, λ is the wavelength of X-ray irradiation, Cu-Kα of wavelength 1.54 Å, β is the full-width half-maximum (FWHM) of the diffraction peak, and θ is the X-ray diffraction angle. The average crystallite sizes of the samples are given in Table 1.

The XRD pattern of undoped TiO_2 shows diffraction peaks at 25.42°, 37.76°, 48.28°, 54.7°, and 62.97° (PDF 86-1157) that correspond to (101), (004), (200), (105), and (204) planes of anatase TiO_2. The XRD pattern of BT1 sample also shows similar peaks, which confirmed that it contains only anatase phase. However, the XRD pattern of BT5 and BT7 sample (doped with 5% and 7% boric acid, respectively) exhibits a peak at 28.11° (PDF 86-0147), which corresponds to (110) plane of rutile phase of TiO_2. This observation is consistent with the previously published report, where rutile phase was observed on increasing the concentration of boron dopant (Chen et al. 2006). Furthermore, it has been reported that rutile content increases when there is an increase in the average

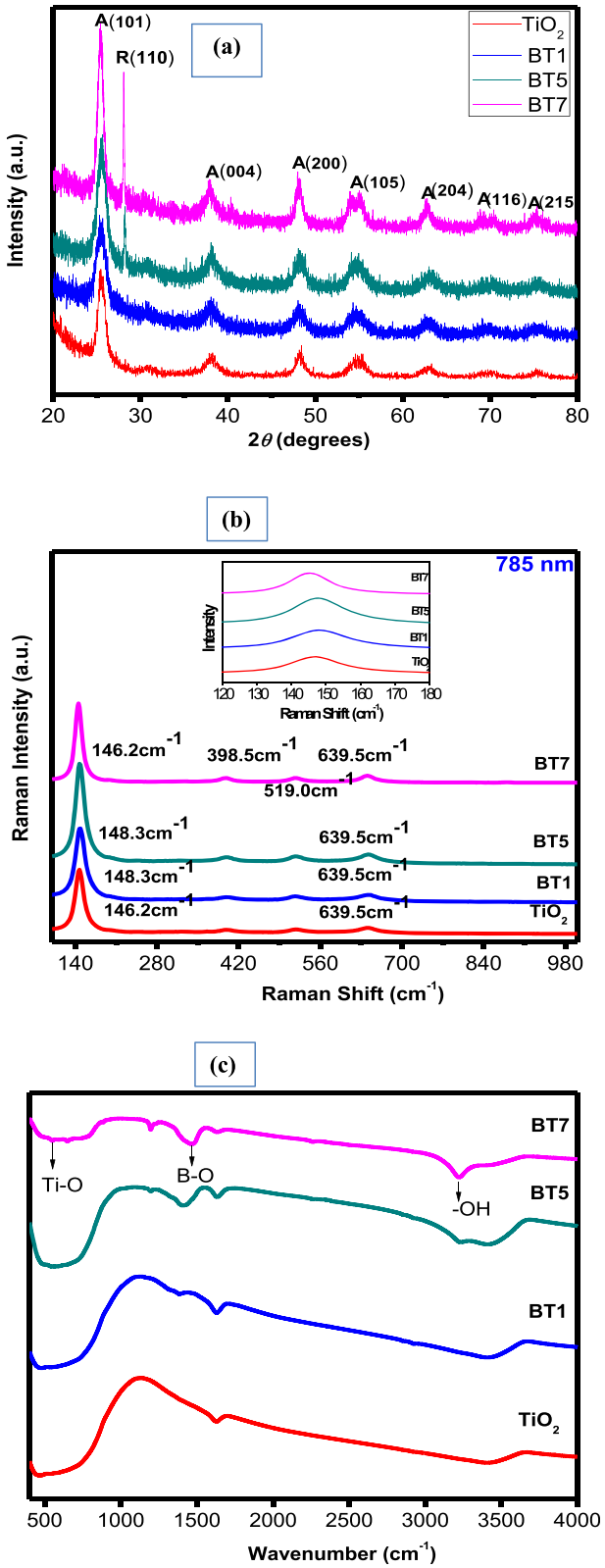

Fig. 1 **a** XRD pattern of undoped TiO_2 and B-doped TiO_2 samples. **b** Raman spectra of undoped TiO_2 and B-doped-TiO_2 samples. **c** FT-IR spectra of undoped TiO_2 and B-doped-TiO_2 samples

Table 1 Surface properties and XRD parameters of undoped TiO_2 and B-TiO_2

Samples	Surface area (m^2/g)	Pore volume (cm^3/g)	Adsorption average pore width (nm)	d spacing (101) plane (Å)	Average crystallite size (nm)
TiO_2	235.47	0.47	8.12	3.49	8.67
BT1	179.11	0.31	6.86	3.50	5.92
BT5	129.51	0.24	7.35	3.48	11.26
BT7	63.30	0.15	9.16	3.50	22.52

crystallite size of the boron-doped samples (Table 1). The appearance of the rutile phase at a higher concentration of boron can be explained due to the structural rearrangement of the catalyst. The anatase to rutile rearrangement involves breaking of two of the six Ti-O bonds in anatase phase (Linsebigler et al. 1995). During the drying process, boron causes the Ti-O-Ti network to weaken, and thus facilitates the Ti-O bond cleavage. Consequently, structural rearrangement may lead to the formation of the rutile phase.

In BT7, a characteristic peak of titanium borate ($TiBO_3$) at 54.08° (PDF 85-0168) was observed, which corresponds to (018) plane. The increase in intensity and sharpening of Bragg peak (101) in BT7 is due to increase in crystal size and improved crystallinity. These results indicate that crystallinity increases due to boron doping. Also, the anatase peak of (101) plane of BT7 shifted to towards lower angle (from 25.50° in TiO_2 to 25.45° in BT7), and thus leads to increase in d-spacing value (Table 1). This suggests that the structure has been modified due to intercalation of boron into the TiO_2 crystal lattice. By doping, the boron may either replace an oxygen atom or occupy an interstitial position in the TiO_2 matrix. The probability that a dopant will substitute oxygen atom depends on its electronegativity. Here, the electronegativity of B (2.04) is much smaller than O (3.44); hence, the possibility of substitution of O with B is ruled out. Likewise, the possibility of substitution of Ti^{4+} with B^{3+} is also very low, because the radius of B^{3+} (0.023 nm) is much smaller than that of Ti^{4+} (0.068 nm). Therefore, it would be difficult for B^{3+} to replace the Ti^{4+} from its site (Chen et al. 2006). Thus, it indicates that boron may occupy the interstitial sites in TiO_2 crystal lattice, thereby modifying the crystal lattice, and hence, variation in d-spacing is observed.

Micro-Raman spectroscopy is one of the most powerful techniques used to investigate the crystalline phase transformations, lattice distortions, oxygen defects, and also the presence of any defect states associated with boron doping into the TiO_2 crystal lattice. Figure 1b shows the micro-Raman spectra recorded in the range of 100–1000 cm^{-1}. The pure TiO_2 (anatase) exhibited six Raman-active modes at wavenumbers 142.5 (E_g), 196 (E_g), 396 (B_{1g}), 515 ($B_{1g} + A_{1g}$), and 640 (E_g) cm^{-1}, respectively (Zhang et al. 2000). It is seen from the Fig. 1b that the E_g band of undoped TiO_2 appeared at 146.2 cm^{-1}. However, the E_g mode is blue shifted (148.3 cm^{-1}) after boron doping at 1% and 5%. This shift after B-doping may be due to the stress induced in the TiO_2 structure upon occupation of interstitial sites by boron, as explained in the XRD studies. However, at 7% boron doping, the peak has again shifted towards lower value (146.2 cm^{-1}). This change in the peak shift may be because of release of stress on increasing the dopant concentration. This indicates that notable modification in structure occurs after the B doping. A blue shift in the anatase E_g peak can be attributed to phonon confinement and oxygen deficiencies (Kafizas and Parkin 2011). Phonon confinement can be caused by several factors, including an expansion in the unit cell volume caused by the introduction of a dopant. Thus, doping results in modification in TiO_2 lattice, which causes broadening of most intense peak in BT7 (inset of Fig. 1b), may contribute to increase in crystallinity. Further, the line shape broadening can be due to tensile stress or defects arise due to doping.

Figure 1c shows the FT-IR spectra of undoped and boron-doped TiO_2. The broad absorption peaks at 3100–3600 cm^{-1} are assigned to stretching vibrations of molecular water and OH groups (Wood et al. 1983). Bands for Ti-O and Ti-O-Ti bonds are observed in the 800–400 cm^{-1} region (Sigaev et al. 2001). The vibrational modes of the borate network are mainly due to the asymmetric stretching relaxation of the B-O bonds of trigonal BO_3 units. Such type of vibrational modes occurs in the range 1200–1750 cm^{-1} with doped samples only (Sharma et al. 2006). Peaks at 1620–1630 cm^{-1} are due to vibrations of hydroxyl groups. In the IR spectra, another peak appears at 1384 cm^{-1}, which can be ascribed to the vibration of tri-coordinated boron (Feng et al. 2011).

HRTEM analysis was performed on undoped TiO_2 and B-TiO_2 (BT7), shown in Fig. 2. Clear high-resolution lattice fringes (Fig. 2a) with a d-spacing of 0.357 nm can be ascribed to the most thermally stable and major anatase (101) facets in undoped TiO_2. Whereas, in BT7 (Fig. 2c), a small increase in d-spacing (0.366 nm) is observed, indicating the interstitial incorporation of boron in the TiO_2 lattice, and hence modification in the structure of TiO_2. TEM images show small pore mesoporous materials with uniform rotundity. After boron doping, both the morphology and crystal structure of TiO_2 are well retained, but the crystallinity is further improved compared to undoped TiO_2. The observations of HRTEM analysis are in agreement with the XRD and Raman data.

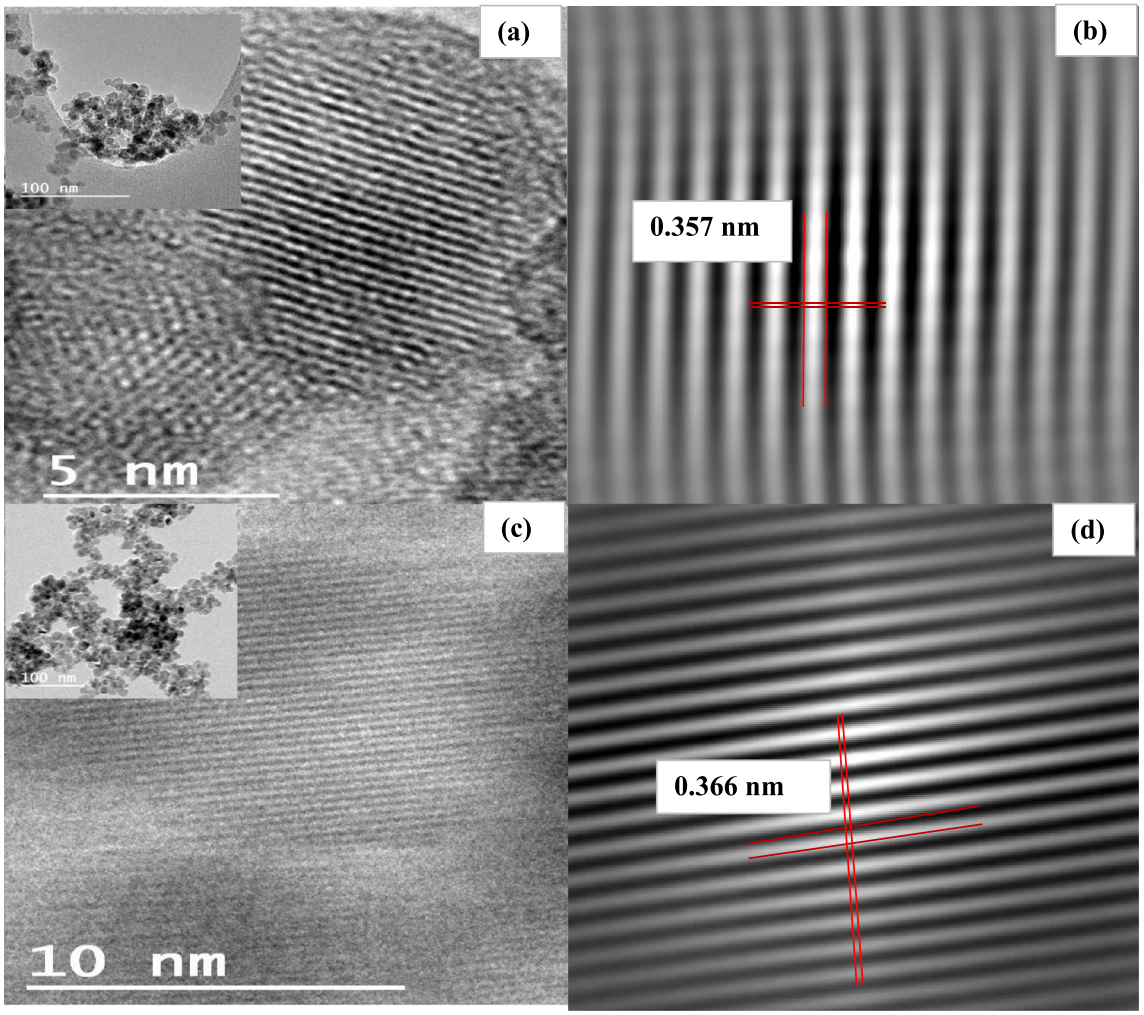

Fig. 2 **a** TEM image of TiO_2 (high resolution) and low resolution [inset]. **b** The distance between the lattice fringes (red parallel lines) pointed by the red arrows is 0.357 nm for TiO_2. **c** TEM images of BT7 (high resolution) and low resolution [inset]. **d** The distance between the lattice fringes (red parallel lines) pointed by the red arrows is 0.366 nm for BT7

Photo-physical properties

The photocatalytic activity of semiconductor material is related to its band gap (E_g). The E_g of prepared materials was evaluated with UV-Vis diffuse reflectance spectroscopy. Figure 3 shows the UV-Vis absorption spectra of the undoped TiO_2 and boron-doped TiO_2 samples. The band gap energy was calculated using following Tauc's relation (Tauc 1970):

$$(\alpha h\nu)^{\S} = \mathrm{A}\left(h\nu - \mathrm{E_g}\right) \quad (2)$$

Where α is absorption coefficient, A is a constant, $h\nu$ is photon energy, and E_g is the optical band gap energy of the material. Figure 1d illustrates the plot of $(\alpha h\nu)^{1/2}$ versus photon energy $(h\nu)$ for pure and boron-doped TiO_2 samples. The E_g values were obtained by extrapolating the linear portion to the photon energy axis. The optical band gap energies of 2.98 eV, 2.98 eV, 2.96 eV, and 2.95 eV were obtained for pure TiO_2, BT1, BT5, and BT7, respectively. These band gap energies were lower than those of commercial TiO_2, which is P25 (3.2 eV). The optical absorption edge of B-doped TiO_2 (BT5 and BT7) is significantly shifted towards visible region when compared to undoped TiO_2. However, no significant differences were found in UV-Vis absorption spectra of BT1 (1 % B-doped TiO_2) as compared to undoped TiO_2. The band-gap values decrease in BT5 and BT7 samples due to the incorporation of B^{3+} ions into TiO_2 crystal lattice and also because of sp-d exchange interactions (Singh et al. 2009). These results suggest that low B content is not sufficient to decrease band gap, however, 5% or higher B content is required to observe optical changes.

Surface/interface properties

The results of surface properties like specific surface area, pore volume, and average pore width of undoped and boron-doped TiO_2 are summarized in Table 1. The specific surface

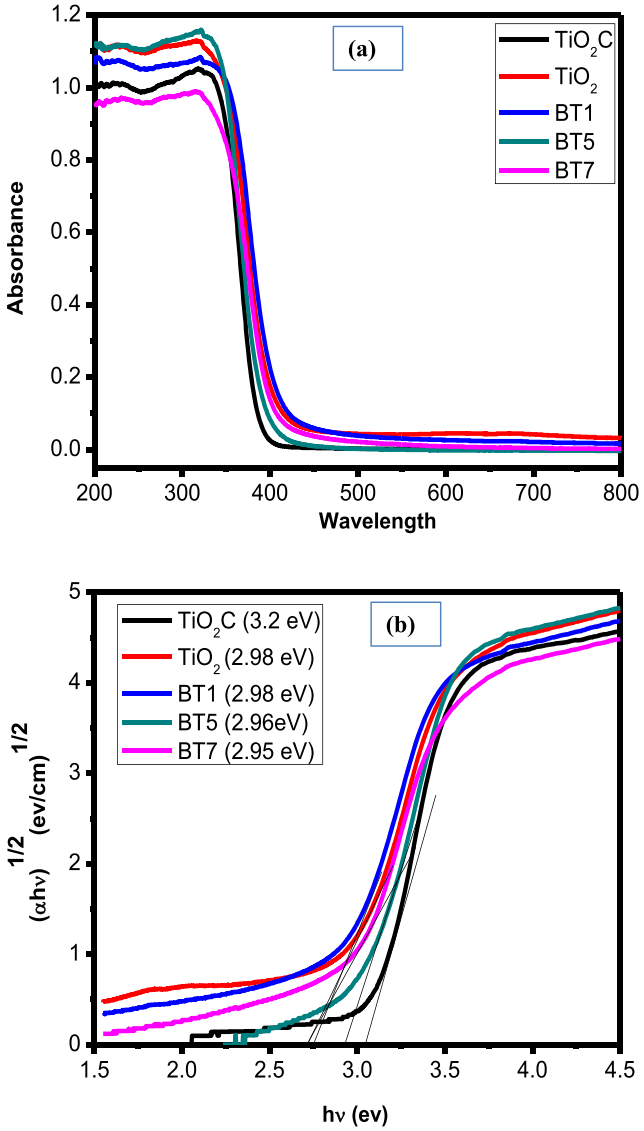

Fig. 3 **a** UV-Vis absorption spectra. **b** Tauc's plot of undoped TiO_2 and B-doped-TiO_2 samples

area and pore volume of TiO_2 decreased with increase in boron content. This may be due to the structure modification and partial pore blockage, caused by boron loading. XRD results indicated that boron occupies the interstitial sites in TiO_2 lattice, and hence, there was an increase in particle size. Moreover, thus, the surface area decreases with increase in particle size (Table 1). These results are in good agreement with observations, as reported by Stengl et al. (2010).

The low-temperature N_2 adsorption-desorption isotherm of undoped and boron-doped TiO_2 is shown in Fig. 4. The samples exhibited a type IV isotherm with an H1-type hysteresis loop associated with open-ended cylindrical pores (Sing et al. 1985). This type of isotherm is a characteristic of mesoporous materials. The inset in Fig. 4 shows the pore size distribution of all the materials. The pore size distribution of BT1 and BT5 shows the presence of mesopores with pore diameter in the

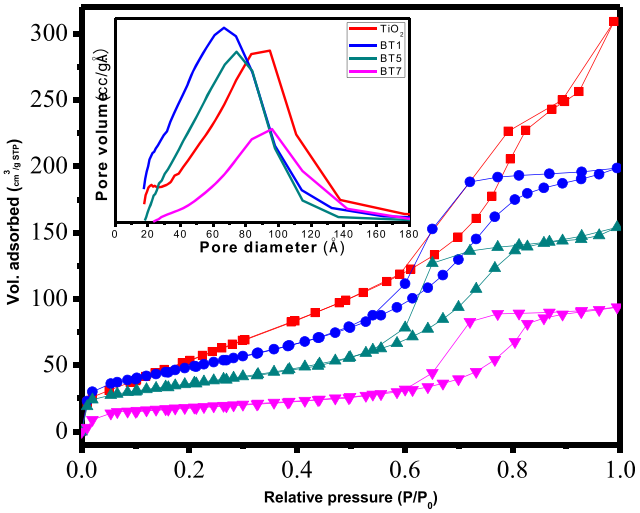

Fig. 4 Low-temperature N_2 adsorption-desorption isotherms and pore size distribution (inset) of undoped TiO_2 and B-doped-TiO_2 samples

range of 2–12 nm, whereas the pore size distributions of TiO_2 and BT7 samples are broad in range (2–15 nm).

The SEM micrographs of TiO_2 and B-doped samples are shown in supporting information as Fig. SI 1. The SEM images showed changes in morphology of TiO_2 after incorporation of boron. For instance, particles of regular size and shape were observed for undoped TiO_2, whereas boron-doped TiO_2 consists of particles of irregular shape and size with a fairly rough surface. In doped samples, the surface with a slightly whitish portion was observed which indicate the deposition of boron dopant. The EDX spectra of microstructures were recorded during SEM imaging and are shown in Fig. 5. It gave both qualitative and quantitative information about the elemental and atomic percentages in undoped TiO_2 and B-doped TiO_2 samples, as presented in Table 2. From EDX results, it is inferred that carbon atom also exists as a dopant in boron-doped sample. It may be due to the reaction of boric acid with carbon present in titanium isopropoxide, forming a complex carbonate species. The EDX results established in situ incorporation of B in TiO_2 lattice with the desired percentage.

To investigate whether these boron atoms doped on the TiO_2 surface, or elsewhere in the lattice structure, the samples were analyzed by XPS, which is a highly surface sensitive technique. The study revealed that B-TiO_2 contains only Ti, O, B, and C elements. The C element can be ascribed to the residual carbon from the precursor solution (TTIP) and the adventitious hydrocarbon from the XPS instrument itself. The binding energies of B, Ti, and O were referenced to the C1s peak (284.6 eV). Figure 6a shows the XPS spectra of the B1s of all doped samples. Usually, B1s electron binding energy peak lies around 188–194 eV. The binding energy (BE) associated with the B1s signal depends on the extent of incorporation of boron atom on TiO_2 surface (In et al. 2007; Gombac et al. 2007). Boron in TiB_2 has BE of 187.5 eV

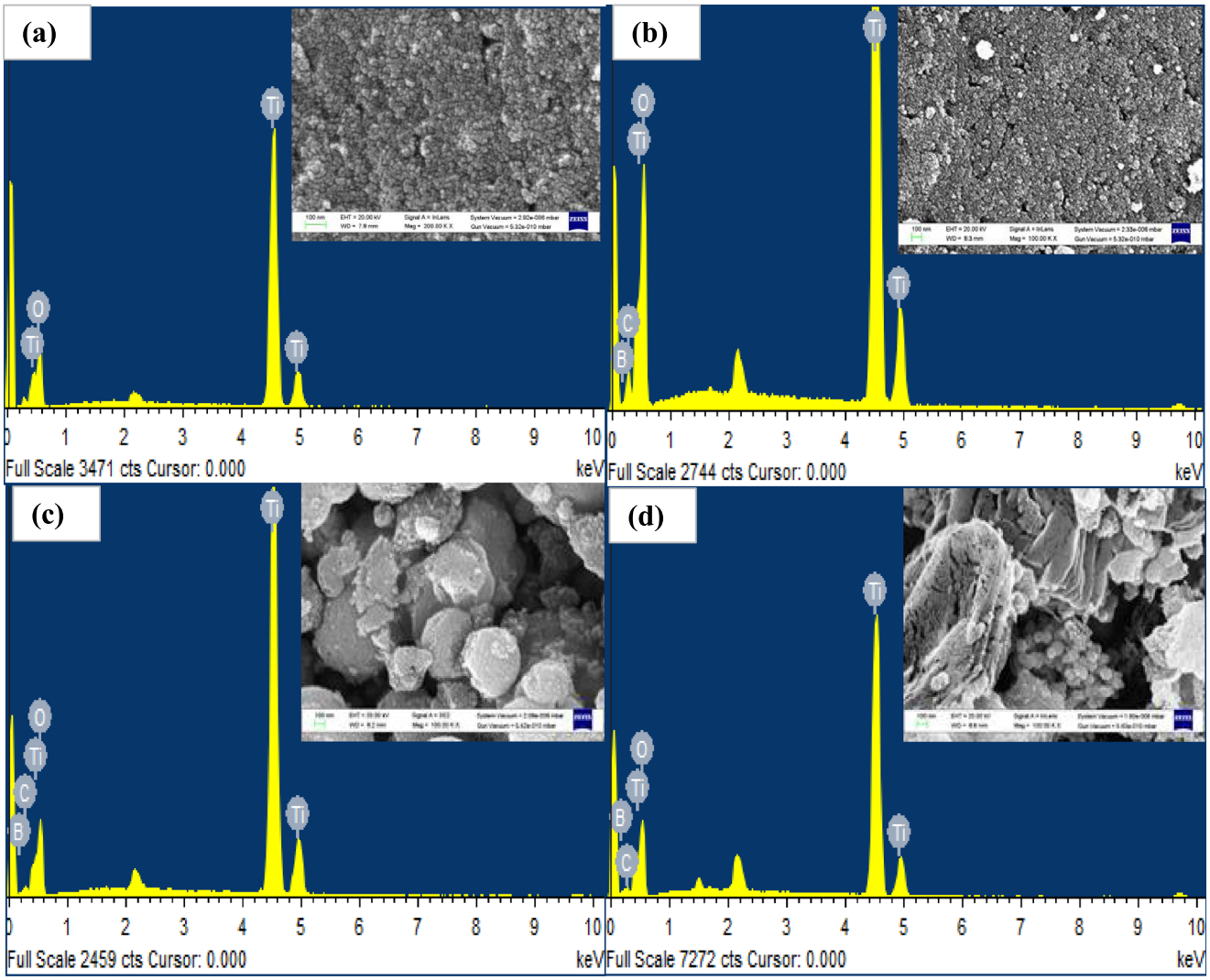

Fig. 5 EDX spectra and SEM images (inset) of (**a**) TiO_2, (**b**) BT1, (**c**) BT5, and (**d**) BT7

(B–Ti bonds) and boron in B_2O_3 or in H_3BO_3 has BE of 193.3 eV (B–O bonds) (Zhu et al. 2007). The binding energy of B1s associated with B substituting O lies around 190.6 eV (Gombac et al. 2007). The peak at around 192 eV corresponds to B1s forming Ti–O–B linkage (Zaleska et al. 2009; Chen et al. 2006; Zhu et al. 2007). Figure 6b shows XPS spectra of Ti2p. The two major peaks at 457.54 eV (Ti $2p_{3/2}$) and 463.2 eV (Ti$2p_{1/2}$) are observed for pure TiO_2. The standard binding energy of Ti$2p_{3/2}$ in TiO_2 for Ti^{3+} is usually located at 457.7 eV, and that for Ti^{4+} is at 459.5 eV (Zhang et al. 2007). XPS peak at 457.54 eV can be ascribed to the formation of Ti^{3+} species, which is shifted to 457.67 eV in boron-doped TiO_2. It indicates that the boron doping favors the formation of surface-layer Ti^{3+} species. Generally, the XPS peak of Ti2p is not broad, and no shoulder peak is observed. However, the TiO_2 surface containing Ti^{3+} results into much broader peak, as seen in doped samples (Fig. 6) (Xiong et al. 2012). The XPS results suggested that B is incorporated at interstitial position in TiO_2, facilitating the formation of Ti^{3+}. Additionally, the existence of Ti^{3+} may result in decrease of recombination of charge carriers (electrons and holes), which influence photocatalytic properties of samples.

Table 2 Catalyst composition TiO_2 and B-TiO_2 catalyst using EDX

Catalyst	Composition (wt %)			
	Ti	O	C	B
TiO_2	52.19	47.81	–	–
BT1	43.59	50.06	5.04	1.30
BT5	52.44	39.71	3.20	4.64
BT7	42.00	44.80	5.65	7.55

Figure 6c shows XPS spectra of O1s. The main O1s component (at around 528 eV) can be ascribed to titanium dioxide (Ti-O), and the second component at around 530 eV which could be due to surface hydroxyl groups (-OH) (Chen et al. 2011). However, the broad O1s region of BT7 can be fitted by three peaks, which are Ti-O in TiO_2, B-O bond, and hydroxyl

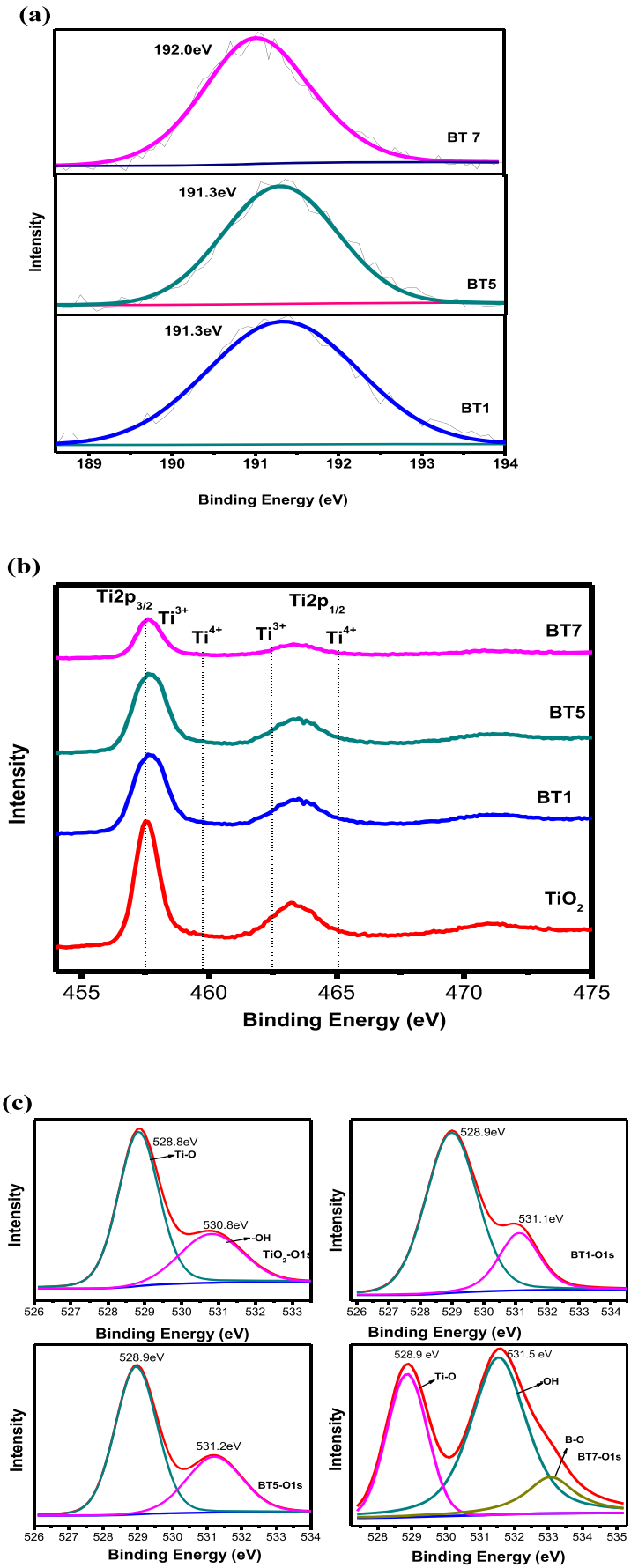

Fig. 6 XPS pattern of (**a**) B1s peaks of B-TiO_2, (**b**) Ti2p peaks of TiO_2, and B-TiO_2. **c** O1s peaks of TiO_2 and B-TiO_2

groups respectively, which further confirms the presence of B-O bond (Chen et al. 2006). The decrease in optical band gap energies with increase in B loading could be due to formation of Ti-O-B-type linkage. Thus, the surface or interfacial properties confirmed the presence of boron into TiO_2 lattice by forming a mesoporous type of nanostructures.

Photocatalytic studies

The effect of catalyst dose on photocatalytic degradation (after 3 h) of 4-NP was investigated to optimize the amount of catalyst. The dose was varied from 0.1 to 1.5 g/L, and the effect of a change in dose on degradation is presented in Fig. 7a. All the prepared materials showed a similar pattern of change in degradation with dose variation. As the concentration of the catalyst in solution was increased, the availability of adsorption sites or active sites was also increased. As a result, the adsorption of 4-NP molecules on the catalyst surface increased and consequently its degradation also get increased from 0.1 to 1.0 g/L of dose.

Further increase in dose did not improve the degradation which is possibly due to following two reasons: (1) aggregation of catalyst particles (Lea and Adesina 2001) and (2) increase in opacity of the solution (Gautam et al. 2006). These observations suggest that the 1.0 g/L dose of the catalyst is optimum dose for degradation of 4-NP. All further experiments were carried out at this dose for the optimization of other experimental variables.

As compared to pure TiO_2, the B-doped TiO_2 catalysts exhibited a significant increase in 4-NP photodegradation efficiency. Figure 7b shows a variation of degradation (C/C_0) as a function of irradiation time in min. It can be observed that

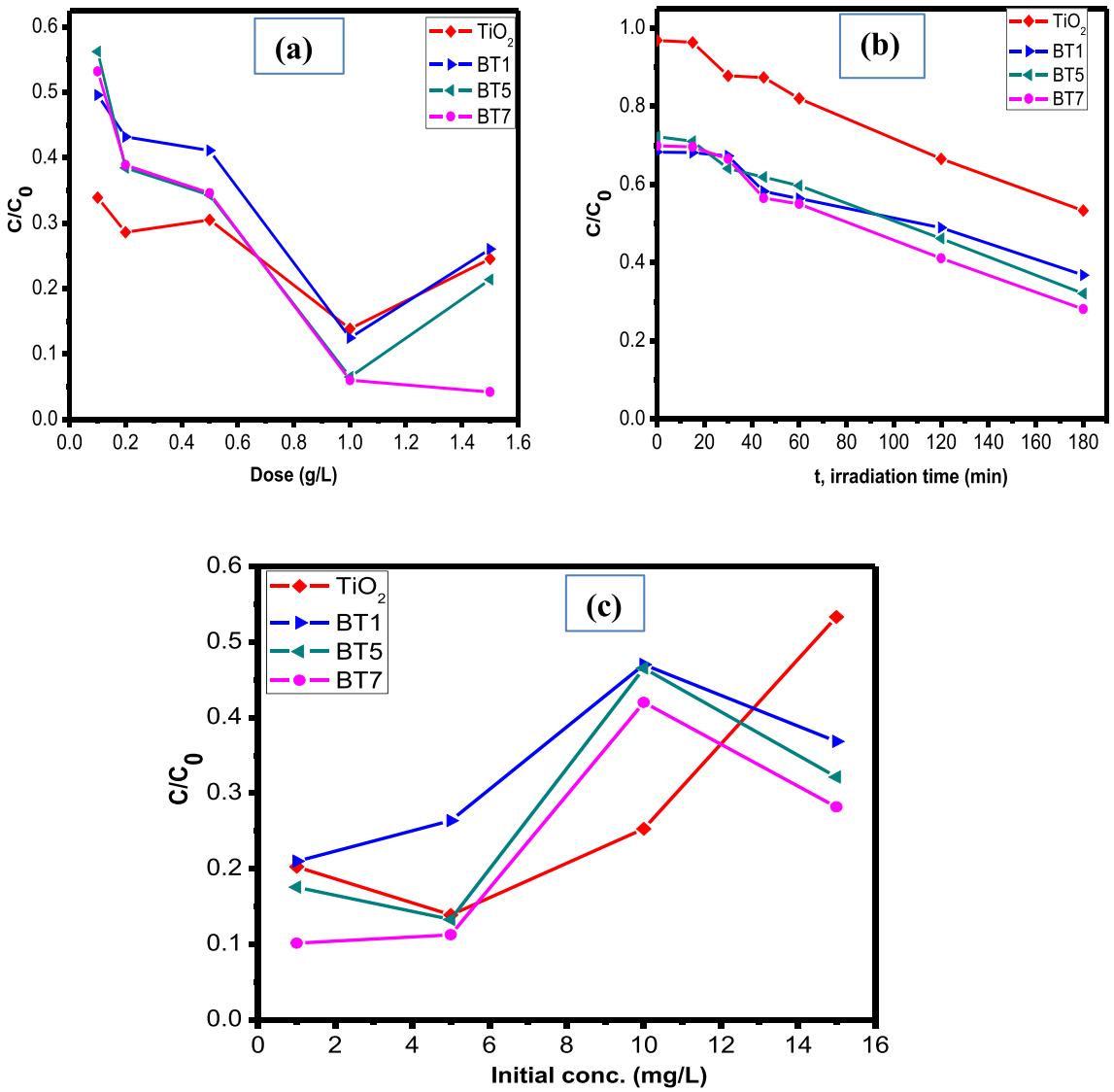

Fig. 7 **a** Effect of catalyst dose on photocatalytic degradation of 4-NP (conc. of 4-NP = 5 mg/L). **b** Effect of boron loading on photocatalytic degradation of 4-NP (conc. of 4-NP = 1 mg/L). **c** Effect of the initial concentration of 4-NP on photodegradation with catalyst dose 1.0 g/L

the presence of boron species positively influences the photocatalytic activity of TiO_2. All the doped samples showed to be more photoactive than undoped TiO_2, where BT7 catalyst, having maximum boron content, showed the highest degradation of a solution containing 15 mg/L of 4-NP.

The pollutant concentration is a critical parameter in any water treatment process, so photocatalytic degradation kinetics was investigated by varying the initial concentration of 4-NP in the range of 1.0 to 15 mg/L. Figure 7c shows the effect of initial concentration of 4-NP solutions on the photocatalytic degradation of 4-NP after irradiation for a fixed duration (180 min). It is evident that with fixed catalyst dose, the increase in initial concentration leads to a gradual decrease in degradation efficiency (C/C_0). It is likely due to the increase in pollutant to catalyst active site ratio. The increase in efficiency was observed after 10 mg/L of initial concentration, particularly with B-doped samples. This observation points towards the possibility of less soluble 4-NP molecules at high concentration. These less soluble molecules get localize on the catalyst surface and get degraded. It is one of the possible reason for an increase in PCD of 4-NP at higher concentration. This phenomenon was not observed in case of as-synthesized TiO_2 (Fig. 7c), which indicates that only B-doped sites encourage the interaction of 4-NP to the surface, and hence, the PCD of TiO_2 is low even at high initial concentration.

Modeling of photocatalytic data

Photocatalytic degradation of 4-NP in the presence of pure and doped TiO_2 is shown in Fig. 8a. Before illumination, the amount of 4-NP adsorbed on the surface of pure TiO_2 is significantly higher than that of B-TiO_2, which is due to higher surface area of pure TiO_2. However, after illumination, the B-TiO_2 (BT7) degraded 90% of 4-NP as compared to 79% degradation by undoped TiO_2. When a small amount of boron (1%) is doped into TiO_2, the photocatalytic activity increases slightly (80%). On further increase in boron content, the activity of BT5 sample also increases (85%) as compared to BT1 and undoped TiO_2. BT7 sample with the highest boron content showed the maximum photocatalytic degradation of 4-NP.

To further explore the kinetics of PCD, first-order rate equation was used, which is as follows:

$$In\left(\frac{C_0}{C}\right) = kt \tag{3}$$

Where, C_0 represents the initial 4-NP concentration in mg/L, C represents remaining 4-NP concentration in mg/L after time t (min) of irradiation, and k is first order rate constant (min^{-1}).

The values of K were obtained from the slope of the graph of $In(C_0/C)$ versus time plot. The BT7 sample showed better photocatalytic activity as compared to all the other samples. Figure 8b gives a comparison of PCD kinetics with all the four samples. The steepness of slope is a measure of rate constant, and hence the photocatalytic activity. It is evident that doping caused an increase in photocatalytic activity with a higher k value. The k values obtained from Fig. 8b are 0.006 min^{-1},0.0109 min^{-1}, 0.0133 min^{-1}, and 0.0322 min^{-1} for TiO_2, BT1, BT5, and BT7, respectively. The post doping increase in PCD is probably due to several factors which are discussed as follows.

Firstly, boron incorporation as a dopant into TiO_2 crystal lattice occupying interstitial sites donates its three valence electrons to the 3d state of titanium ions, according to the process (Finazzi et al. 2009):

$$B + 3Ti^{4+} \rightarrow B^{3+} + 3Ti^{3+}$$

The existence of a reduced form of Ti^{3+} on the surface of TiO_2 (as evidence from XPS) is responsible for enhancement

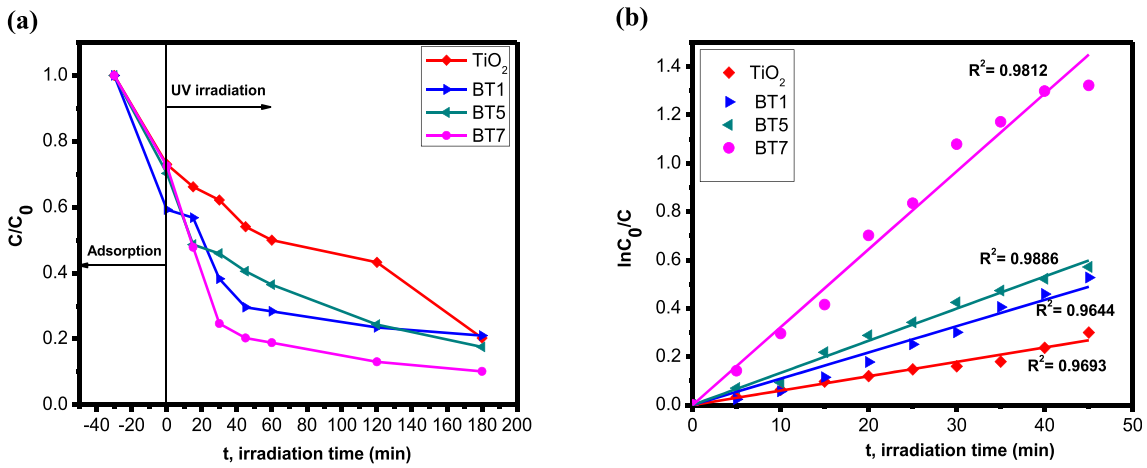

Fig. 8 **a** Photocatalytic degradation of 4-NP in presence of undoped and B-TiO_2. **b** First-order rate plot of photocatalytic degradation of 4-NP under UV irradiation in presence of undoped and B-TiO_2 (catalyst dose 1.0 g/L, 4-NP conc. 1 mg/L)

Table 3 Comparison of prepared TiO_2 and B-TiO_2 catalyst with other photocatalysts for degradation of 4-NP under different conditions

S. No.	Band gap (eV)	% degradation	Photocatalyst	Light irradiation conditions	Concentration of 4-NP	Rate constant (k) in min^{-1}	Ref.
1.	2.4	73.8 98.1	Ag-N-P tridoped TiO_2	UV Visible	Not reported	Not reported	Achamo and Yadav 2016
2.	Not reported	87	C,N-TiO_2 photocatalyst	Simulated sunlight irradiation	7.0×10^{-2} mM	4.87×10^{-3}	Osin et al. 2018
3.	Not reported	49.5	Graphene modified TiO_2	Simulated sunlight irradiation	10 mg/L	0.021	Liu et al. 2017
4.	Not reported	90	Commercial TiO_2 (P25)	UV	1.0×10^{-4} M	Not reported	Islam et al. 2014
5.	3.05	99.9	N,S-TiO_2	Visible	2 mg/L	0.0302	Rahimi et al. 2012
6.	Not reported	99.9	CuPp–TiO_2 + H_2O_2 photocatalyst	Visible	10^{-4} mol/L	Not reported	Yao et al. 2012
7.	2.95 2.98	90 79	B-TiO_2 photocatalyst Pure TiO_2	UV	1 mg/L	0.0322 0.006	Our work

in photocatalytic activity. It might act as an active site to assist the adsorption of reactant and trap the photogenerated charge carriers (electrons and holes), and therefore may reduce their recombination. Secondly, it is well known that the specific surface area and the anatase phase plays a significant role in the photocatalytic activity of TiO_2 (Zhou et al. 2005). A large surface area plays an important role in any photocatalytic degradation reactions, as a large number of organic molecules may get adsorbed on the catalyst surface, and thus promotes the reaction rate (Kim et al. 2009). However, powders with the large surface area are usually associated with more crystalline defects, which favor the possibility of recombination of photogenerated charge carriers, leading to a poor photocatalytic activity (Carp et al. 2004). Therefore, the sufficient surface area is a requirement, but not a determinant factor for a photocatalyst. The surface area of boron-doped samples is less than that of pure TiO_2.

The decrease in the specific surface area and pore diameters due to the presence of boron was reported in the literature (Stengl et al. 2010). The BET surface area tends to decrease with increase in boron content, which indicated the presence of mesopores as evidenced by the pore size distribution. The photocatalytic activity of amorphous TiO_2 is negligible, also indicates that crystallinity is another important requirement (Zhou et al. 2005; Anpo et al. 1987). So, a balance between specific surface area and crystallinity is a very important factor in determining the photocatalytic activity of the TiO_2 material. The XRD, Raman, and BET results suggest that BT7 possess good anatase phase, crystallinity, and optimum surface area, which results in its better photocatalytic activity. In addition, narrowing of the band gap (2.95 eV) compared to undoped TiO_2 (2.98 eV) caused increase in the photocatalytic activity of BT7. Also, the existence of Ti-O-B linkage, evidenced from XPS, has synergistic effect on the photocatalytic activity of the B-doped TiO_2 (BT7). The photodegradation results of present study were compared with results of previous studies involving photo-catalytic degradation of 4-NP using different catalyst or conditions. Table 3 shows this comparison on the parameters like % degradation, band-gap, photo catalyst, and radiation type, concentration, and rate constants. It is evident, from this comparison, that photocatalytic efficiency of B-doped photo catalyst is comparable/and even better than some of the co-doped TiO2 catalyst. The rate constant of B-doped TiO2 based 4-NP degradation is reasonably high as compared to other photo catalysts.

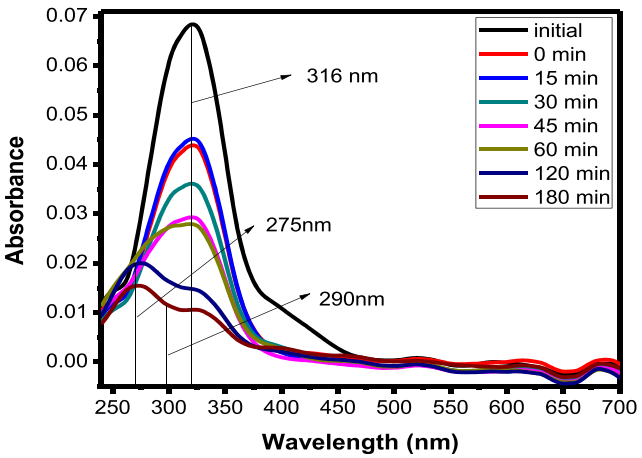

Fig. 9 Photocatalytic degradation of 4-NP monitored by UV-Vis spectroscopy in presence of B-TiO_2

Mechanism of PCD of 4-NP

Figure 9 shows the absorption spectral changes as a function of time during photocatalytic degradation of 4-NP, in the presence of B-TiO_2. The changes in absorption peaks of 4-NP were monitored with UV-Vis spectrophotometer. The

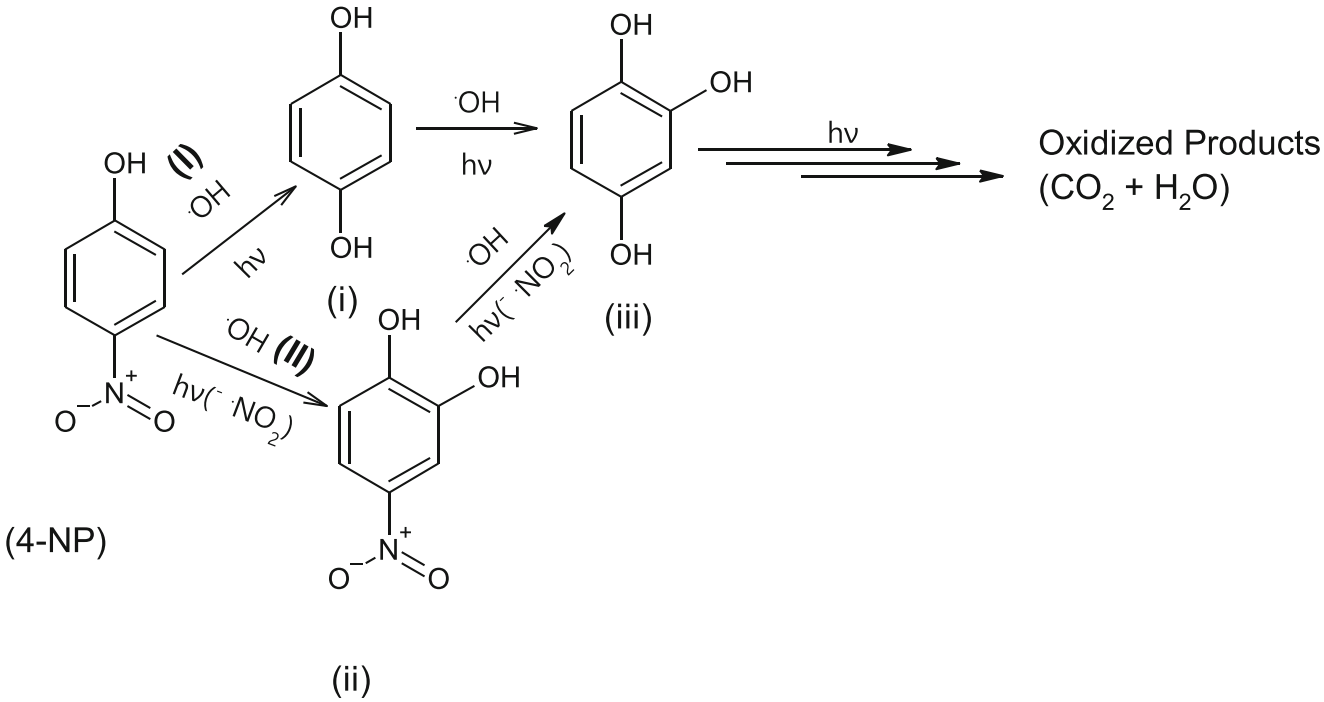

Scheme 1 Expected chemical oxidation pathway of 4-NP degradation during illumination in presence of B-TiO_2 [(i) benzoquinone, (ii) 4-nitro catechol and (iii) 1,2,4-trihydroxy benzene]

UV-Vis spectra of reaction mixtures of 4-NP at different reaction times show observable changes as the photocatalytic degradation proceeds. Before degradation, 4-NP shows a sharp characteristic absorption band at λ_{max} 316 nm, as evidenced in spectra of initial sample taken. After short irradiation times (15–30 min), this absorption band gets decreased in intensity. Then, after prolonged irradiation (120–180 min), the absorption band at 316 nm disappears along with emergence of two new bands at λ_{max} 275 nm and 290 nm. The appearance of these bands is most likely due to the formation of intermediate degradation products, hydroquinone (λ_{max} 290 nm) and 1,2,4-trihydroxy benzene (λ_{max} 275 nm) (Edgar et al. 2012). In literature, previous studies also reported these degradation products as oxidation intermediates of 4-NP (Nevim et al. 2002; Won-Young et al. 2007). The photocatalytic reactions involve generation of ·OH radicals, which are electrophilic in nature. The nitro group in 4-NP is a very good leaving group and can be eliminated easily by an electrophilic substitution of the ·OH radicals at the para position with respect to the hydroxyl group. It further forms, hydroxylated products (hydroquinone and 1,2,4-trihydroxy benzene) by following two different pathways, through hydrogen abstraction and subsequent addition or substitution to the formed radicals as shown in Scheme 1. On the basis of absorption band spectra, it is expected that the degradation of 4-NP is following first pathway. Further, oxidation of degradation products leads to complete mineralization into carbon dioxide and water molecule (Di Paola et al. 2003).

Conclusions

Here, a single step, facile sol-gel synthesis of undoped and B-doped TiO_2 nanostructures with various B loadings (1, 5, 7% w/v) is reported. XRD and HRTEM results showed that B doping has improved crystallinity, and doped catalysts contained a mixture of anatase and rutile phase. The 5% B (BT5) or higher amount (BT7) caused significant changes in the structure as evidenced by increase in average crystallite size and average pore width; however, not much appreciable change was observed with low B (1%) content. In addition, the band gap was decreased to 2.96 eV and 2.95 eV for BT5 and BT7, respectively as compared to undoped TiO_2 (2.98 eV). XPS studies revealed that boron occupies interstitial sites in TiO_2 crystal lattice by forming a Ti-O-B type linkage. Photocatalytic degradation of 4-NP with various B loadings was monitored and catalyst with highest B content (BT7) exhibited maximum degradation efficiency (90%) as compared to undoped TiO_2 (79%). The formation of Ti-O-B type bond has synergistic effect on enhancing the photocatalytic activity. Thus, these results have clearly demonstrated that the photocatalytic properties of B-TiO_2 catalysts depend on the amount of B loading and it is a deciding factor in determination of structural, interfacial, and photo-physical properties. The B-TiO_2 catalysts could be a potential material for decomposition of organic contaminants from industrial wastewater samples.

Acknowledgments The authors are grateful to Dr. R. K. Singh, Indian Institute of Petroleum, CSIR, Dehradun, for providing assistance in UV-Vis DRS and FTIR study. Author Vandana Yadav is thankful to University Grants Commission for her doctoral grant (NFO-2015-17-OBC-UTT-29056) which provided the impetus needed to carry out this work.

References

Achamo T, Yadav OP (2016) Removal of 4-nitrophenol from water using Ag–N–P tridoped TiO_2 by photocatalytic oxidation technique. Anal Chem Insights 11:29–34

Ali F, Khan SB, Kamal T, Anwar Y, Alamry KA, Asiri AM (2017a) Antibacterial chitosan/zinc phthalocyanine fibers supported metallic and bimetallic nanoparticles for the removal of organic pollutants. Carbohydr Polym 173:676–689

Ali F, Khan SB, Kamal T, Anwar Y, Alamry KA, Asiri AM (2017b) Bactericidal and catalytic performance of green nanocomposite based-on chitosan/carbon black fiber supported monometallic and bimetallic nanoparticles. Chemosphere 188:588–598

Ali F, Khan SB, Kamal T, Anwar Y, Alamry KA, Bakhsh EM, Asiri AM, Sobahi TRA (2018) Synthesis and characterization of metal nanoparticles templated chitosan-SiO_2 catalyst for the reduction of nitrophenols and dyes. Carbohydr Polym 192:217–230

Anpo M, Shima T, Kodama S, Kubokawa Y (1987) Use of visible light second-generation TiO_2 photocatalysts quantization effects and reaction intermediates. J Phys Chem 91:4305–4310

Byrne C, Subramanian G, Pillai SC (2018) Recent advances in photocatalysis for environmental applications. J Environ Chem Eng 6(3):3531–3555

Carp O, Huisman CL, Reller A (2004) Photoinduced reactivity of titanium dioxide. Prog Solid State Chem 32:33–177

Chen DM, Yang D, Wang Q, Jiang ZY (2006) Effects of boron doping on photocatalytic activity and microstructure of titanium dioxide nanoparticles. Ind Eng Chem Res 45:4110–4116

Chen XQ, Zhang XW, Lei LC (2011) Electronic structures and photocatalysis properties under visible irradiation of F-doped TiO_2 nanotube arrays. J Inorg Mater 26:369–374

Chio W, Termin A, Hoffman MR (1994) The role of metal ion dopants in quantum-sized TiO_2: correlation between photoreactivity and charge carrier recombination dynamics. J Phys Chem 98:13669–13679

Di Paola A, Augugliaro V, Palmisano L, Pantaleo G, Savinov E (2003) Heterogeneous photocatalytic degradation of nitrophenols. J Photochem Photobiol A Chem 155:207–214

Edgar M, Elisa L, Claudia AA, Raúl AL, Carlos M (2012) Photocatalytic degradation of paracetamol: intermediates and total reaction mechanism. JHazard Mater 243:130–138

Ellappan P, Miranda L, Synthesis R (2014) Characterization of cerium doped titanium catalyst for the degradation of nitrobenzene using visible light. Inter J Photoenergy 756408, 9 pages

Fakhri A, Behrouz S (2015a) Assessment of SnS_2 nanoparticles properties for photocatalytic and antibacterial applications. Sol Energy 117:187–191

Fakhri A, Behrouz S (2015b) Photocatalytic properties of tungsten trioxide (WO_3) nanoparticles for degradation of lidocaine under visible and sunlight irradiation. Sol Energy 112:163–168

Fakhri A, Kahi DS (2017) Synthesis and characterization of MnS_2/reduced graphene oxide nanohybrids for with photocatalytic and antibacterial activity. J Photochem Photobiol B Biol 166:259–263

Fakhri A, Khakpour R (2015) Synthesis and characterization of carbon or/and boron-doped CdS nanoparticles and investigation of optical and photoluminescence properties. J Lumin 160:233–237

Fakhri A, Naji M (2017) Degradation photocatalysis of tetrodotoxin as a poison by gold doped PdO nanoparticles supported on reduced graphene oxide nanocomposites and evaluation of its antibacterial activity. J Photochem Photobiol B Biol 167:58–63

Fakhri A, Nejad PA (2016) Antimicrobial, antioxidant and cytotoxic effect of molybdenum trioxide nanoparticles and application of this for degradation of ketamine under different light illumination. J Photochem Photobiol B Biol 159:211–217

Fakhri A, Pourmand M, Khakpour R, Behrouz S (2015) Structural, optical, photoluminescence and antibacterial properties of copper-doped silver sulfide nanoparticles. J Photochem Photobiol B Biol 149:78–83

Fakhri A, Rashidi S, Tyagi I, Agarwal S, Gupta VK (2016) Photodegradation of erythromycin antibiotic by γ-Fe_2O_3/SiO_2 nanocomposite: response surface methodology modeling and optimization. J Mol Liq 214:378–383

Feng N, Zheng AM, Wangetal Q (2011) Boron environments in B-doped and (B, N)-codoped TiO_2 photocatalysts: a combined solid-state NMR and theoretical calculation study. J Phys Chem C 115:2709–2719

Finazzi E, Di Valentin C, Pacchioni G (2009) Boron-doped anatase TiO2: pure and hybrid DFT calculations. J Phys Chem C 113:220–228

Gautam S, Kamble SP, Sawant SB, Pangarkar VG (2006) Photocatalytic degradation of 3 nitrobenzene sulfonic acid in aqueous TiO_2 suspensions. J Chem Technol Biotechnol 81:359–364

Gombac V, De Rogatis L, Gasparotto A, Vicario G, Montini T, Barreca D, Balducci G, Fornasiero P, Tondello E, Graziani M (2007) TiO_2 nanopowders doped with boron and nitrogen for photocatalytic applications. Chem Phys 339:111–123

Haider S, Kamal T, Khan SB, Omar M, Haider A, Khan FU, Asiri AM (2016) Natural polymers supported copper nanoparticles for pollutants degradation. Appl Surf Sci 387:1154–1161

Hamadanian M, Reisi-Vanani A, Majedi A (2009) Preparation and characterization of S-doped TiO_2 nanoparticles, effect of calcination temperature and evaluation of photocatalytic activity. Mater Chem Phys 116:376–382

Hashimoto K, Irie H, Fujishima A (2005) TiO_2 photocatalysis: a historical overview & future prospects. Jap J Appl Phys 44:8269–8285

Hassani A, Khataee A, Karaca S, Fathinia M (2016) Heterogeneous photocatalytic ozonation of ciprofloxacin using synthesized titanium dioxide nanoparticles on a montmorillonite support: parametric studies, mechanistic analysis and intermediates identification. RSC Adv 6:87569–87583

Hassani A, Khataee A, Fathinia M, Karaca S (2018a) Photocatalytic ozonation of ciprofloxacin from aqueous solution using TiO_2/MMT nanocomposite: nonlinear modeling and optimization of the process via artificial neural network integrated genetic algorithm. Process Saf Environ Prot 116:365–376

Hassani A, Eghbali P, Ekicibil A, Metin O (2018b) Monodisperse cobalt ferrite nanoparticles assembled on mesoporous graphitic carbon nitride ($CoFe_2O_4$/mpg-C_3N_4): a magnetically recoverable nanocomposite for the photocatalytic degradation of organic dyes. J Magn Magn Mater 456:400–412

Hong XT, Wang ZP, Cai WM, Lu F, Zhang J, Yang YZ, Ma N, Liu Y (2005) Visible-light-activated nanoparticle photocatalyst of iodine-doped titanium dioxide. J Chem Mater 17:1548–1552

In S, Orlov A, Berg R, García F, Pedrosa-Jimenez S, Tikhov MS, Wright DS, Lambert RM (2007) Effective visible light-activated B-doped and B,N-codoped TiO_2 photocatalysts. J Am Chem Soc 129:13790–13791

Islam S, Bormon SK, Hossain MNK, Habib A, Islam TSA (2014) Photocatalytic degradation of p-nitrophenol (PNP) in aqueous suspension of TiO_2. Am J Anal Chem 5:483–489

Kafizas A, Parkin IP (2011) Combinatorial atmospheric pressure chemical vapor deposition (cAPCVD): a route to functional property optimization. J Am Chem Soc 133:20458–20467

Kamal T, Ahmad I, Khan SB, Asiri AM (2019a) Bacterial cellulose as support for biopolymer stabilized catalytic cobalt nanoparticles. Int J Biol Macromol 135:1162–1170

Kamal T, Ali F, Ahmad I, Asiri AM, Khan SB (2019b) Chitosan-coated polyurethane sponge supported metal nanoparticles for catalytic reduction of organic pollutants. Int J Biol Macromol 132:772–783

Kavitha V, Palanivelu K (2005) Degradation of nitrophenols by Fenton and photo-Fenton processes. J Photochem Photobiol A Chem 170: 83–95

Khan FU, Asimullah, Khan SB, Kamal T, Asiri AM, Khan IU, Akhtar K (2017) Novel combination of zero-valent Cu and Ag nanoparticles @ cellulose acetate nanocomposite for the reduction of 4-nitro phenol. Int J Biol Macromol 102:868–877

Kim E, Kim DS, Ahn B (2009) Synthesis of mesoporous TiO_2 and its application to photocatalytic activation of methylene blue and E. coli. Bull Kor Chem Soc 30:193–198

Kumaravel V, Mathew S, Bartlett J, Pillai SC (2019) Photocatalytic hydrogen production using metal doped TiO_2: a review of recent advances. Appl Catal B Environ 244:1021–1064

Lea J, Adesina AA (2001) Oxidative degradation of 4-nitrophenol UV illuminated TiO_2 suspension. J Chem Technol Biotechnol 76:803–810

Linsebigler AL, Lu G, Yates JT (1995) Photocatalysis on TiO_2 surfaces: principles, mechanisms, and selected results. Chem Rev 95:735–758

Liu X, Zhao L, Lai H, Li S, Yi Z (2017) Efficient photocatalytic degradation of 4-nitrophenol over graphene modified TiO_2. J Chem Technol Biotechnol 92:2417–2424

May-Lozano M, Ramos-Reyes GM, López-Medina R, Martínez-Delgadillo SA, Flores-Moreno J, Hernández-Pérez I (2014) Effect of the amount of water in the synthesis of B-TiO_2: Orange II photodegradation. Inter J Photochem 2014:721216 8 pages

Mohammadi S, Sohrabi M, Golikand AN, Fakhri A (2016) Preparation and characterization of zinc and copper co-doped WO_3 nanoparticles: application in photocatalysis and photobiology. J Photochem Photobiol B Biol 161:217–221

Nevim S, Arzu H, Gülin K, Zekiye Ç (2002) Photocatalytic degradation of 4-nitrophenol in aqueous TiO_2 suspensions: theoretical prediction of the intermediates. J Photochem Photobiol A Chem 146:189–197

Osin OA, Yu T, Cai X, Jiang Y, Peng G, Cheng X, Li R, Qin Y, Lin S (2018) Photocatalytic Degradation of 4-Nitrophenol by C, N-TiO_2: Degradation efficiency vs. embryonic toxicity of the resulting compounds. Front Chem 6(92):1–9

Park H, Choi W (2004) Effects of TiO_2 surface fluorination on photocatalytic reactions and photoelectrochemical behaviors. J Phys Chem B 108:4086–4093

Rahimi R, Rabbani M, Moghaddam SS (2012) Comparison of photocatalysis degradation of 4-nitrophenol using N,S co-doped TiO_2 nanoparticles synthesized by two different routes. J Sol-Gel Sci Technol 64:17–26

Ren W, Ai Z, Jia F, Zhang L, Fan X, Zou Z (2007) Low temperature preparation and visible light photocatalytic acitivity of mesoporous carbon-doped crystalline TiO_2. Appl Catal B 69:138–144

Scherrer P (1918) *Gottinger Nachrichten* Gesell. 2:98

Sharma G, Singh K, Priya M, Mohan S, Singh H, Bindra S (2006) Effects of gamma irradiation on optical and structural properties of PbO-Bi_2O_3-B_2O glasses. Radiat Phys Chem 75:959–966

Shipra G, Manoj T (2011) A review of TiO_2 nanoparticles. Chin Sci Bull 56:1639–1657

Sigaev VN, Pernice P, Aronne A, Akimova OV, Stefanovich SY, Scagline A (2001) $KTiOPO_4$ precipitation from potassium titanium phosphate glasses, producing second harmonic generation J. Non-Cryst Solids 92:59–69

Sing KSW, Everet DH, Haul RAW, Moscou L, Pierotti RA, Rouquerol J, Siemieniewska T (1985) Reporting physisorption data for gas/solid systems with special reference to the determination of surface area and porosity. Pure Appl Chem 57:603–619

Singh P, Kumar A, Kaur D (2009) Mn-doped ZnO nanocrystalline thin films prepared by ultrasonic spray pyrolysis. J Alloys Compd 471: 11–15

Stengl V, Housková V, Bakardjieva S, Murafa N (2010) Photocatalytic activity of boron-modified TiO_2 under UV and visible-light illumination. Appl Mater Interfaces 2:575–580

Tauc J (1970) Absorption edge and internal electric fields in amorphous semiconductors. Mater Res Bull 5:721–730

U.S. Environmental Protection Agency (1980) 4-Nitrophenol, health and environmental effects Profile No. 135, Washington DC

Viswanathan B, Krishanmurthy KR (2012) Nitrogen incorporation in TiO_2: does it make a visible light photoactive material. Inter J Photoenergy (ID 269654)1–10

Ward MD, Bard AJ (1982) Photocurrent enhancement via trapping of photogenerated electrons of TiO_2 particles. J Phys Chem 86:3599–3605

Won-Young A, Sarah AS, Tijana R, Donald MC (2007) Photocatalytic reduction of 4-nitrophenol with arginine-modified titanium dioxide nanoparticles. Appl Catal B Environ 74:103–110

Wood DL, Rabinovich EM, Johnson DW Jr, Mac-Chesney JB, Vogel EM (1983) Preparation of high-silica glasses from colloidal gels. 3. Infrared spectrophotometric studies. J Am Ceram Soc 66:693–699

Xiong LB, Li JL, Yang B, Yu Y (2012) Ti^{3+} in the surface of titanium dioxide: generation, properties and photocatalytic application. J Nanomater 2012:831524 13 pages

Xu JJ, Ao YH, Chen MD, Fu DG (2009) Low temperature preparation of boron-doped TiO_2 by hydrothermal method and its photocatalytic activity. J Alloys Compd 484:73–79

Yao GP, Li J, Luo Y, Sun WJ (2012) Efficient visible photodegradation of 4-nitrophenol in the presence of H_2O_2 by using a new copper(II) porphyrin–TiO_2 photocatalyst. J Mol Catal A Chem 361–362:29–35

Zaleska A, Sobczak JW, Grabowska E, Hupka J (2008) Preparation and photocatalytic activity of boron-modified TiO_2 under UV and visible light. Appl Catal B Environ 78:92–100

Zaleska A, Grabowska E, Sobczak JW, Gazda M, Hupka J (2009) Photocatalytic activity of boron-modified TiO_2 under visible light: the effect of boron content, calcination temperature and TiO_2 matrix. Appl Catal B Environ 89:469–475

Zhang WF, He YL, Zhang MS, Yin Z, Chen Q (2000) Raman scattering study on anatase TiO_2 nanocrystals. J Phys D Appl Phys 33:912–916

Zhang YG, Ma LL, Li JL, Yu Y (2007) In situ Fenton reagent generated from TiO2/CuO2 composite film: a new way to utilize TiO_2 under visible light irradiation. Environ Sci Technol 41:6264–6269

Zhang W, Yang B, Chen J (2012) Effects of calcination temperature on preparation of boron-doped TiO_2 by sol-gel method. Inter J Photoenergy 2012:528637 8 pages

Zhou MH, Yu JG, Cheng B, Yu HG (2005) Preparation and photocatalytic activity of Fe-doped mesoporous titanium dioxide nanocrystalline photocatalysts. Mater Chem Phys 93:159–163

Zhu J, Yang J, Bian ZF, Ren H, Liu YM, Cao Y, Li HX, He HY, Fan KN (2007) Nanocrystalline anatase TiO_2 photocatalysts prepared via a facile low temperature nonhydrolytic sol–gel reaction of $TiCl_4$ and benzyl alcohol. Appl Catal B 76:82–91